

1 **Implementation of state-of-the-art ternary new particle formation scheme** 2 **to the regional chemical transport model PMCAMx-UF in Europe**

3
4 E. Baranizadeh¹, B. N. Murphy^{2,3}, J. Julin^{1,2}, S. Falahat^{2,4}, C. L. Reddington⁵, A. Arola⁶, L. Ahlm², S.
5 Mikkonen¹, C. Fountoukis⁷, D. Patoulias⁸, A. Minikin⁹, T. Hamburger¹⁰, A. Laaksonen^{1,11}, S. N.
6 Pandis^{8,12,13}, H. Vehkamäki¹⁴, K. E. J. Lehtinen^{1,6}, I. Riipinen²

7
8 ¹Department of Applied Physics, University of Eastern Finland, Kuopio, Finland

9 ²Department of Environmental Science and Analytical Chemistry (ACES), Stockholm University,
10 Stockholm, Sweden

11 ³Now at the National Exposure Research Laboratory, US Environmental Protection Agency, Research
12 Triangle Park, USA

13 ⁴Now at the Swedish Meteorological and Hydrological institute (SMHI), Norrköping, Sweden

14 ⁵Institute for Climate and Atmospheric Science, School of Earth and Environment, University of Leeds,
15 Leeds, UK

16 ⁶Finnish Meteorological Institute, Kuopio, Finland

17 ⁷Qatar Environment and Energy Research Institute (QEERI), Hamad Bin Khalifa University (HBKU),
18 Qatar Foundation, Doha, Qatar

19 ⁸Department of Chemical Engineering, University of Patras, Patras, Greece

20 ⁹German Aerospace Agency DLR, Oberpfaffenhofen, Germany

21 ¹⁰Norwegian Institute for Air Research (NILU), Oslo, Norway

22 ¹¹Climate research Unit, Finnish Meteorological Institute, Helsinki, Finland

23 ¹²Institute of Chemical Engineering Sciences, Foundation for Research and Technology Hellas
24 (ICEHT/FORTH), Patras, Greece

25 ¹³Department of Chemical Engineering, Carnegie Mellon University, Pittsburgh, PA, USA

26 ¹⁴Division of Atmospheric Sciences, Department of Physics, University of Helsinki, Helsinki, Finland

27 28 **Abstract**

29 The particle formation scheme within PMCAMx-UF, a three dimensional chemical transport model,
30 was updated with particle formation rates for the ternary H₂SO₄-NH₃-H₂O pathway simulated by the
31 Atmospheric Cluster Dynamics Code (ACDC) using quantum chemical input data. The model was
32 applied over Europe for May 2008, during which the EUCAARI-LONGREX campaign was carried out
33 providing aircraft vertical profiles of aerosol number concentrations. The updated model reproduces the
34 observed number concentrations of particles larger than 4 nm within one order of magnitude throughout
35 the atmospheric column. This agreement is encouraging considering the fact that no semi-empirical
36 fitting was needed to obtain realistic particle formation rates. The cloud adjustment scheme for

37 modifying the photolysis rate profiles within PMCAMx-UF was also updated with the TUV
38 (Tropospheric Ultraviolet and Visible) radiative-transfer model. Results show that although the effect
39 of the new cloud adjustment scheme on total number concentrations is small, enhanced new particle
40 formation is predicted near cloudy regions. This is due to the enhanced radiation above and in the
41 vicinity of the clouds, which in turn leads to higher production of sulfuric acid. The sensitivity of the
42 results to including emissions from natural sources is also discussed.

43

44 **1 Introduction**

45 Formation of new particles from atmospheric vapors (new particle formation, NPF) is potentially an
46 important source of particulate matter in the atmosphere, especially in the ultrafine (<100 nm in
47 diameter) size range (Kulmala et al., 2004; Merikanto et al., 2009; Jung et al., 2010; Fountoukis et al.,
48 2012; Kerminen et al., 2012; Fuzzi et al., 2015). In the past, in modeling studies on the role of in-situ
49 NPF as a particle source, particle formation has been represented with various parameterizations
50 including binary (Vehkamäki et al., 2002) or ternary (Napari et al., 2002) nucleation based on the
51 classical nucleation theory (CNT), semi-empirical activation (Kulmala et al., 2006), kinetic (McMurry,
52 1980) or organic-enhanced (Paasonen et al., 2010) NPF and/or ion-mediated nucleation (Yu and Luo,
53 2009). These parameterizations have generally assumed sulfuric acid (H₂SO₄), water (H₂O), ammonia
54 (NH₃), or different organic species as the compounds forming the new particles. The activation, kinetic
55 and organic-enhanced mechanisms are semi-empirical, based on the observed dependence of particle
56 formation rates on concentrations of sulfuric acid and/or organic vapors (Sihto et al., 2006; Paasonen et
57 al., 2010). The advantage of such methods is that they are simple and produce nucleation rates of the
58 same order as those observed. However, as they are fit to specific experiments usually at ground level,
59 they are most reliable at locations and conditions similar to those at which the data has been obtained.
60 The ternary H₂SO₄-H₂O-NH₃ parameterization by Napari et al. (2002) has been used with some success
61 (Jung et al., 2008; Jung et al., 2010; Fountoukis et al., 2012; Westervelt et al., 2014), but with quite
62 drastic correction factors necessary to reproduce ambient particle number concentrations. In many
63 previous studies (Spracklen et al., 2006; Makkonen et al., 2009; Yu et al., 2010) the binary H₂SO₄-H₂O
64 nucleation has been assumed to dominate in the upper atmosphere and be negligible at lower altitudes,
65 and it has often been superimposed with one of the other mechanisms.

66

67 Sulfuric acid, water and ammonia have long been established as important molecules forming new
68 particles in the atmosphere (Korhonen et al., 1999; Kulmala et al., 2000; Laaksonen et al., 2008).
69 However, standard theoretical descriptions of the ternary H₂SO₄-H₂O-NH₃ particle formation pathway
70 have not been able to reproduce measured particle formation rates – hence the need to resort to semi-
71 empirical parameterizations and correction factors to describe this process in atmospheric models.
72 Recent experimental (Kirkby et al., 2011; Almeida et al., 2013; Jen et al., 2014) and computational

73 developments have, however, changed this picture drastically. Flexible computational models (such as
74 the Atmospheric Cluster Dynamics Code, ACDC, Olenius et al., 2013) which simulate the kinetics of a
75 population of molecular clusters combined with cluster free energies calculated from first-principles
76 methods, can now reproduce laboratory observations of particle formation rates in $\text{H}_2\text{SO}_4\text{-NH}_3$ as well
77 as H_2SO_4 -amine systems with reasonable accuracy (Almeida et al., 2013), without the need for empirical
78 scaling of the predicted particle formation rate.

79
80 Predictions of particle number concentration from regional-scale chemical transport models have been
81 evaluated typically with data from ground-level observations (Jung et al., 2008; Matsui et al., 2011,
82 2013; Fountoukis et al., 2012; Cui et al., 2014; Lupascu et al., 2015). Meanwhile, there is much to gain
83 from assessing the model against vertically resolved particle number observations, as many of the
84 uncertainties in the model relate to particle scavenging, by hydrometeors as well as other particles, and
85 mixing of air masses. The possible biases introduced from parameterizing new particle formation rates
86 with ground-level data makes it all the more imperative to evaluate and constrain models with
87 observations taken at altitude. Recent studies (Reddington et al., 2011; Matsui et al., 2013; Lupascu et
88 al., 2015) have begun assessing global- and regional-scale models in this way against data from
89 European, Asian and US field campaigns involving aircraft measurements. Furthermore, it is worthwhile
90 to explore the vertical variability in chemical and environmental precursors to NPF (e.g. H_2SO_4 , NH_3 ,
91 T , RH , etc.) and particle number concentrations.

92
93 In this work we describe the implementation of a $\text{H}_2\text{SO}_4\text{-H}_2\text{O-NH}_3$ new particle formation scheme based
94 on the output of the ACDC model to the regional chemical transport model PMCAMx-UF (Jung et al.,
95 2010, Fountoukis et al., 2012). We test the new scheme by simulating the evolution of atmospheric gas-
96 phase and aerosol particle concentrations during May 2008 in Europe. We evaluate the model against
97 ground-based and airborne observations of aerosol particle number size distributions during the
98 simulated period. Furthermore, we implement an updated radiative-transfer scheme TUV (Tropospheric
99 Ultraviolet and Visible radiative-transfer model; Madronich, 2002) for PMCAMx-UF and discuss its
100 implications for predictions of NPF and particle number concentrations in the European domain.

101

102 **2 Methods**

103 **2.1 PMCAMx-UF model description**

104 PMCAMx-UF is a three-dimensional regional chemical transport model that simulates both the size-
105 dependent particle number and chemically resolved mass concentrations (Jung et al. 2010). PMCAMx-
106 UF utilizes the framework of the air quality model PMCAMx (Gaydos et al., 2007, Karydis et al., 2007),
107 where the description of vertical and horizontal advection and dispersion, wet and dry deposition, and

108 gas-phase chemistry are based on the CAMx air quality model, and the variable size-resolution model
109 of Fahey and Pandis (2001) is used for aqueous-phase chemistry. To treat the aerosol microphysics,
110 including NPF, condensation and coagulation, PMCAMx-UF uses the Dynamic Model for Aerosol
111 Nucleation (DMAN) module by Jung et al. (2006). DMAN uses the Two-Moment Aerosol Sectional
112 (TOMAS) algorithm (Adams and Seinfeld, 2002) to track the aerosol number and mass distributions.
113 DMAN divides the aerosol particles into 41 logarithmically-spaced size bins between 0.8 nm and 10
114 μm .

115
116 The aerosol species modeled in PMCAMx-UF include sulfate, ammonium, water, elemental carbon,
117 crustal material, chloride, sodium, nitrate, primary organic aerosol and four secondary organic aerosol
118 surrogate compounds. The version of TOMAS used in the model applied here tracks explicitly the mass
119 transfer of sulfate and ammonium while that of water is treated assuming equilibrium. Within the
120 DMAN aerosol microphysics module the remaining compounds are represented by inert surrogate
121 species. The pseudo-steady-state approximation method (Pierce and Adams, 2009), which assumes
122 steady-state concentration for sulfuric acid, is used for the calculation of NPF and sulfuric acid
123 condensation rates. The condensation of ammonia is calculated independently following the approach
124 described in Jung et al. (2006).

125
126 New particle formation rates in the standard version of PMCAMx-UF have been calculated in previous
127 studies using a scaled version of the ternary $\text{H}_2\text{SO}_4\text{-NH}_3\text{-H}_2\text{O}$ parametrization by Napari et al. (2002),
128 hereafter referred to as the “scaled” Napari parameterization. The original Napari parameterization is
129 based on predictions of the CNT assuming that the energetics of the molecular clusters follow bulk
130 thermodynamics. While it has been shown to perform better than a range of other nucleation
131 parameterizations in predicting the occurrence of new particle formation events (Jung et al. 2008), it is
132 also known to overpredict ultrafine particle number concentrations (Gaydos et al., 2005; Yu et al., 2006;
133 Jung et al., 2006; Merikanto et al., 2007b; Zhang et al., 2010). Thus a semi-empirical correction factor
134 of 10^{-6} has been applied previously in PMCAMx-UF to scale the formation rates produced by the Napari
135 parameterization and better match the observations (Jung et al., 2010; Fountoukis et al., 2012; Ahlm et
136 al., 2013).

137
138 Encouraged by the good agreement between particle formation rates predicted by the ACDC model and
139 the state-of-the-art experimental data (Almeida et al., 2013), we have updated the particle formation
140 scheme within PMCAMx-UF with ACDC-based particle formation rates for the $\text{NH}_3\text{-H}_2\text{SO}_4\text{-H}_2\text{O}$ (see
141 Sect. 2.2 for details and the Results section for comparison to the scaled Napari parameterization). In
142 addition to applying the ternary $\text{H}_2\text{SO}_4\text{-NH}_3\text{-H}_2\text{O}$ NPF scheme, we also include a binary $\text{H}_2\text{SO}_4\text{-H}_2\text{O}$
143 NPF pathway. This pathway is operating simultaneously with the ternary pathway and is based on the
144 Vehkamäki et al. (2002) CNT-parameterization.

145

146 PMCAMx-UF was applied for the period of May 2008 for the European domain which consists of a
147 $5400 \times 5832 \text{ km}^2$ region with a $36 \times 36 \text{ km}^2$ grid resolution and 14 vertical layers reaching an altitude
148 of approximately 20 km. The PMCAMx-UF output data are hourly averaged. The meteorological inputs,
149 described in detail in Fountoukis et al. (2011; 2012), were created using the Weather Research and
150 Forecasting model version 2 (Skamarock et al., 2005) and include horizontal wind components, vertical
151 dispersion coefficients, temperature, pressure, water vapor mixing ratios, cloud optical depths and
152 rainfall rates. Hourly gridded emissions include anthropogenic emission rates of primary particulate
153 matter and gases. For the particle emissions the Pan-European anthropogenic Particle Number Emission
154 Inventory (Denier van der Gon et al., 2009; Kulmala et al., 2011) and the Pan-European Carbonaceous
155 Aerosol Inventory (Kulmala et al., 2011) were used. The anthropogenic gas emissions include both land
156 emissions from the GEMS data set (Visschedijk et al., 2007) and international shipping emissions. These
157 emission inputs are the same as have been used previously for the May 2008 period in PMCAMx-UF
158 (in Fountoukis et al., 2012; Ahlm et al., 2013), and thus in order to enable comparison to the previous
159 works these inputs are used in all of the base model runs of the present paper. To assess how much the
160 particle number concentrations are affected by emissions from natural sources we have performed
161 simulations with and without these emissions. The natural emissions include both particulate matter and
162 gases and combine three different datasets: emissions from ecosystems based on the MEGAN model
163 (Guenther et al., 2006), marine emissions based on the model of O'Dowd et al. (2008), and wildfire
164 emissions (Sofiev et al., 2008a, b).

165

166 **2.2 Improved treatment of the ternary NPF pathway**

167 The ternary $\text{H}_2\text{SO}_4\text{-NH}_3\text{-H}_2\text{O}$ particle formation rate at approximately 1.3 nm in mobility diameter was
168 calculated with the Atmospheric Cluster Dynamics Code (ACDC; Olenius et al., 2013; Almeida et al.,
169 2013; Henschel et al., 2015). ACDC simulates the dynamics of a population of molecular clusters by
170 numerically solving the cluster birth–death equations. Instead of considering only collisions and
171 evaporations of single vapor molecules, an often-used assumption applied in the CNT framework,
172 ACDC allows all possible collision and fragmentation processes within the cluster population. As input
173 the ACDC code needs the corresponding rate constants, of which the most challenging to assess are the
174 cluster evaporation rates, generally calculated from the free energies of formation of the clusters. The
175 evaporation rates play a significant role in determining the number concentration and consequently the
176 formation rate of small particles. The liquid drop model, commonly used in CNT to calculate the free
177 energies of cluster formation, is based on macroscopic thermodynamics and is thus not expected to give
178 reliable results for small clusters (Merikanto et al., 2007a). Among the most important of additional
179 uncertainties is representing the energetics of the system with bulk thermodynamics e.g. assuming
180 complete proton-transfer which is known not to hold for small clusters and results in drastic errors in

181 the formation free energies and internally inconsistent handling of small stable ammonia-sulfuric acid
182 clusters. The most accurate theoretical method to compute the free energies of clusters consisting of
183 specific molecules is quantum chemistry. This modeling approach is able to reproduce the general trends
184 in cluster formation, and leads to, thus far, the best quantitative agreement between observations and
185 modeling with no fitting parameters (Almeida et al., 2013). Having a description that has been evaluated
186 against laboratory data and has e.g. temperature- and RH-dependencies in line with the current
187 theoretical understanding gives a new capacity for e.g. extrapolating back to the pre-industrial
188 atmosphere for which we have very little observational data (see e.g. Carslaw et al., 2013; Kirkby et al.,
189 2016).

190
191 In the ACDC simulations of this work, hard-sphere collision rates were used for the collision rate
192 coefficients, and the evaporation rate coefficients were calculated from the Gibbs free energies of
193 formation of the clusters computed with quantum chemical methods at the B3LYP/CBSB7//RICC2/aug-
194 cc-pV(T+d)Z level (Ortega et al., 2012; Henschel et al., 2014). This level of theory has been tested
195 against higher level methods and was shown to give reliable cluster formation free energies at an
196 affordable computational cost. The simulation included clusters containing up to three H₂SO₄ and three
197 NH₃ molecules, hydrated by up to four or five water molecules. Sulfuric acid and ammonia were
198 explicitly treated in the simulation, and water was implicitly included by assuming that the clusters are
199 in equilibrium with respect to water and by using hydrate averaged collision and evaporation rates. An
200 external sink term corresponding to scavenging by larger particles was used for all the clusters. The
201 steady-state particle formation rate was obtained as the flux of clusters growing out of the simulation
202 system considering boundary conditions based on cluster stability. Details of the simulated ternary
203 H₂SO₄-NH₃-H₂O system can be found in Henschel et al. (2015).

204
205 The ACDC results were implemented in the PMCAMx-UF framework as a look-up table consisting of
206 a comprehensive set of particle formation rates computed at different values of H₂SO₄ and NH₃
207 concentrations, temperature, RH, and coagulation loss rate due to scavenging by the population of
208 larger particles (described by the condensation sink, see e.g. Dal Maso et al., 2002). The formation rate
209 data produced by theoretical models have been traditionally fitted to a multivariable functional form
210 (Napari et al., 2002; Merikanto et al., 2007b), with the resulting parameterization then utilized by large-
211 scale models. However, finding a suitable functional form to cover satisfactorily the whole parameter
212 space becomes increasingly difficult with increasing number of input parameters, with increasing
213 number of species participating in NPF, and with the tendency of formation rates to exhibit rapid, step
214 function-like changes with respect to one or more parameters. Thus interpolating from a look-up table
215 provides formation rates that are more closely in line with the original theoretical model, with a relatively
216 minor additional computational cost. The parameter space encompasses sulfuric acid concentration
217 between $1.00 \cdot 10^4$ and $3.16 \cdot 10^9$ molecules cm⁻³, ammonia concentration between 10^6 and 10^{11}

218 molecules cm^{-3} , relative humidity between 0 and 100 %, temperature between 180 and 320 K and
219 condensation sink between 10^{-5} and 10^{-1} s^{-1} . These conditions bound the environmental and chemical
220 conditions predicted by typical PMCAMx-UF runs for Europe in May. PMCAMx-UF uses multilinear
221 interpolation to extract formation rates from the look-up table. The newly formed particles are added to
222 the second lowest size bin of PMCAMx-UF, corresponding to the size for which the ACDC formation
223 rates were calculated. This approach provides PMCAMx-UF with formation rates that are based on the
224 full kinetic treatment of the cluster population.

225

226 **2.3 Radiative-transfer and photolysis rates**

227 Aerosols and clouds can enhance or reduce photolysis of relevant gas-phase chemical species in the
228 atmosphere by reflecting, scattering, or absorbing solar radiation. Modifications of photolysis rates via
229 this interaction lead to changes in the production rate of sulfuric acid, which lead directly to changes in
230 the new particle formation rates. Previous versions of PMCAMx-UF employed a parameterization
231 originally used by the Regional Acid Deposition Model (RADM; Chang et al., 1987) to treat the
232 modification of photolysis rates due to cloud presence. This approach required the cloud optical depth
233 from the meteorological input data and the solar zenith angle in order to calculate the time- and layer-
234 dependent adjustment factors for the photolysis rates. This method, however, did not use aerosol
235 concentrations predicted online by the transport model. Instead, a reference aerosol profile was used for
236 every time step and column of grid cells.

237

238 To more realistically treat the effects of clouds on the photolysis rates profile of the atmospheric column,
239 we updated the online approach in PMCAMx-UF to a streamlined form of the two-stream radiative-
240 transfer module, TUV (Tropospheric Ultraviolet and Visible radiative-transfer model; Madronich,
241 2002). The implementation of TUV was completed as documented by Emery et al. (2010). This
242 simplified module employs a reduced number of wavelength bands and plane-parallel two-stream
243 approximations. Inputs needed include the cloud optical depth, solar zenith angle, three-dimensional
244 aerosol concentration profile, and optical properties of the aerosol components provided by Takemura
245 et al., 2002.

246

247 The total cloud optical depth τ above a current grid cell to the top of troposphere is approximated offline
248 by

$$249 \quad \tau = \frac{3L\Delta z_c}{2\rho_w r}, \quad (1)$$

250 where L is the mean cloud liquid water (g m^{-3}), Δz_c is the mean depth of cloudy layer (m) in the cell, ρ
251 is the density of water (10^6 g m^{-3}), and r is the mean cloud-drop radius (10^{-5} m). The module also uses

252 the time- and space-dependent vertical profile of dry and wet (with an RH-dependent lensing effect)
253 aerosols predicted by PMCAMx-UF.

254

255 The module outputs a modified actinic flux that can then be applied, using the clear-sky actinic flux for
256 reference, to adjust the clear-sky photolysis rates. Adjustments due to clouds and aerosols tend to reduce
257 photolysis below clouds but often enhance rates above clouds because of the reflection from the top of
258 the cloud. Emery et al. (2010) implemented the module in the Comprehensive Air Quality Model with
259 Extensions (CAMx) and evaluated it for ozone prediction in the Houston area. That study found
260 decreased ozone surface concentrations with maximum decreases of approximately 10 ppb. However,
261 they did not report the impacts that the radiation feedback would have on particulate mass or number.
262 We compare particle number and sulfuric acid vapor profiles with and without the radiation update in
263 place to better understand the importance of correctly representing this phenomenon.

264

265 **2.4 Model evaluation with particle number and size distribution data**

266 During the European Aerosol Cloud Climate and Air Quality Interactions (EUCAARI) project (Kulmala
267 et al., 2009; 2011) particle number size distributions within the atmospheric boundary layer were
268 measured at various European Supersites for Atmospheric Aerosol Research (EUSAAR). May 2008
269 was one of the intensive observation periods of the project. In this study the predicted ground-level
270 hourly averaged particle number concentrations are evaluated against the data from Aspvreten
271 (Sweden), Cabauw (Netherlands), Hyytiälä (Finland), Ispra (Italy), Mace Head (Ireland), Melpitz
272 (Germany) and Vavihill (Sweden) similarly to Fountoukis et al. (2012). These locations represent seven
273 different types of European environments (Ahlm et al., 2013). More information about the
274 characteristics and topography of these sites is available elsewhere (Asmi et al., 2011 and Fountoukis et
275 al., 2012). The particle size distribution measurements were carried out using either a Differential
276 Mobility Particle Sizer (DMPS) or Scanning Mobility Particle Sizer (SMPS) systems in the mobility
277 diameter size range above 10 nm.

278 To evaluate the vertical profile of the particle size distribution, we used the observational data measured
279 by the German DLR Falcon 20 and the British FAAM BAe-146 research aircrafts, operating between 6
280 and 24 May 2008. The aircraft data was collected during the LONGREX campaign (Hamburger et al.,
281 2011), which was also a part of the EUCAARI project. The FAAM BAe-146 flights mainly flew in the
282 boundary layer and lower free troposphere while the DLR Falcon 20 aircraft mostly probed the free
283 troposphere up to the tropopause level (Hamburger et al., 2011). The Condensation Particle Size
284 Analyser (CPSA) (Fiebig et al., 2005; Feldpausch et al., 2006), installed aboard the DLR Falcon 20, and
285 the Passive Cavity Aerosol Spectrometer Probe (PCASP-100X) (Liu et al., 1992), operated aboard both
286 aircraft, measured the particle number concentrations. Consistent with Reddington et al. (2011), we used
287 the measurements from two channels of the CPSA onboard the DLR Falcon 20 with lower cut-off

288 diameters of 4 and 10 nm, yielding the number concentrations of particles above these sizes, denoted as
289 N_4 and N_{10} . The temporal resolution of the CPSA dataset is 1 s. The nominal size range of PCASP-100X
290 is 0.12-3.5 μm with 15 channels. The PCASP-100X raw data was sampled with 1 Hz frequency, but the
291 data used here is based on averaging over a constant interval of 5 s. We used the measured particle
292 number concentrations obtained from channels 3 to 10 of the PCASP-100X covering the diameter range
293 of 160-1040 nm, representative of the accumulation mode, also to facilitate comparisons with the results
294 reported by Reddington et al. (2011). We also used a TSI 3786 Condensational Particle Counter (CPC)
295 aboard the FAAM BAe-146 aircraft to measure the number concentrations of particles larger than 4 nm.

296 A map of flight tracks by the Falcon 20 and BAe-146 and more details about EUCAARI-LONGREX
297 dataset are available elsewhere (Reddington et al., 2011; Hamburger et al., 2012). Measurements from
298 the LONGREX campaign span altitudes corresponding to 13 of the 14 vertical layers of PMCAMx-UF
299 (Fig. S1 in the supplement). The model data were paired with the aircraft data by converting the time-
300 dependent latitude, longitude, and altitude of the plane to a model grid-cell index.

301 **3 Results**

302 **3.1 Surface-level particle number concentrations**

303 In this study we explore the sensitivity of PMCAMx-UF to cases (1) with an updated NPF scheme with
304 ACDC-based formation rates, (2) with an updated cloud adjustment scheme with TUV implementation,
305 and (3) including natural particle number emissions. The baseline simulation (hereafter ACDC-TUV-
306 DE; see Table 1) represents a prediction of the particle number concentrations with implementation of
307 ACDC-based NPF scheme and TUV cloud adjustment scheme while using the default (i.e. only
308 anthropogenic) particle emissions similarly to Fountoukis et al. (2012). Table 1 summarizes the
309 simulations reported in this study. Figure 1 shows the arithmetic mean number concentration over May
310 2008 at ground-level for each PMCAMx-UF grid cell for particles larger than 10 (N_{10}), 50 (N_{50}) and 100
311 (N_{100}) nm and all particles (N_{tot}) as predicted using the baseline simulation ACDC-TUV-DE. The first
312 two days of the simulation were excluded from the analysis to minimize the impact of the initial
313 conditions on the results. The domain mean during May 2008 for N_{tot} is 59200 cm^{-3} , for N_{10} the
314 corresponding number is 7100 cm^{-3} , for N_{50} 1300 cm^{-3} , and for N_{100} 360 cm^{-3} . The spatial pattern of the
315 predicted number concentrations is similar to the results reported by Fountoukis et al. (2012), which
316 were obtained using the simulation Napari-RADM-DE. The highest number concentrations are
317 predicted over Eastern Europe during this photochemically active period while the lowest particle
318 number concentrations are predicted over Nordic countries. The simulation Napari-TUV-DE predicts
319 the domain mean of N_{tot} , N_{10} , N_{50} and N_{100} of 8100, 4000, 1500 and 410, respectively. Although updating
320 the NPF scheme of PMCAMx-UF with ACDC-based formation rates significantly affects the number
321 of small particles with diameter below 10 nm, the spatial concentration remains unchanged. Updating

322 the model cloudiness scheme by implementing the TUV radiative-transfer module did not greatly affect
323 the spatial distribution of number concentrations but caused a minor change in the number concentration
324 values. This is confirmed by the arithmetic domain mean values during May 2008 of N_{tot} , N_{10} , N_{50} and
325 N_{100} predicted by the ACDC-RADM-DE simulation, which are 62000, 6800, 1200 and 340 cm^{-3} ,
326 respectively, and thus very similar to the baseline simulation. Including the natural particle emissions
327 (in simulation ACDC-TUV-NE) resulted in 48300, 6200, 1300 and 380 cm^{-3} for N_{tot} , N_{10} , N_{50} and N_{100} ,
328 respectively, therefore predicting lower number concentrations of small particles (i.e. diameter < 10 nm)
329 compared to that predicted by the baseline simulation. This is probably due to the higher sink of newly
330 formed particles caused by the added natural particle emissions.

331
332 Figure 2 shows scatter plots of the predicted (ACDC-TUV-DE) versus measured hourly averaged N_{10} ,
333 N_{50} and N_{100} at the seven EUSAAR measurement sites during May 2008. The prediction skill metrics of
334 the simulations presented in Table 1 as compared with surface observations are summarized in
335 Supplementary Table S1. The model generally tends to overpredict the N_{10} (NMB = 126 % for the base
336 simulation) and the predicted N_{10} are subject to scatter (NME = 145 % for the base simulation) (see
337 Table S1 for all the simulations). The reason for this overprediction is most likely linked to the missing
338 condensable vapors and particle growth mechanisms in the simulations reported here (see Fountoukis et
339 al., 2012; Ahlm et al., 2013; Patoulias et al., 2015). At most of the measurement sites, the predicted N_{50}
340 is in fairly-good agreement with the observations with about 70% of the data points falling within a
341 factor of two of the measurements except for two sites Mace Head (56%) and Hyytiälä (59%) (see Fig.
342 2 for the base simulation). The N_{50} predictions are overall slightly biased (NMB = -18 % for the base
343 simulation) but subject to scatter (NME = 41 % for the base simulation). The predicted N_{100} are more
344 biased (NMB = -45%) and scattered (NME = 51 %) compared with N_{50} . Overall, the model performance
345 is comparable to that reported by Fountoukis et al., (2012) and between the five simulations conducted
346 here, with largest differences observed for the smallest particles if the scaled Napari scheme is used (see
347 Table S1): linear correlation coefficients for monthly average concentrations throughout the domain
348 between the different simulation cases and the ACDC-TUV-DE range from 0.827 (for N_{tot} for Napari-
349 TUV-DE vs. the base case) to 0.999 (for N_{tot} and N_{100} for ACDC-RADM-DE vs. the base case). As
350 expected, including the natural emissions resulted in better agreement with the observations as compared
351 with the default case, especially for the small sizes (see Table S1 for comparison between ACDC-TUV-
352 NE and ACDC-TUV-DE).

353
354 The biases presented here and in the following figures can thus be considered conservative estimates.
355 Furthermore, in this study we have only considered the ternary sulfuric acid - water - ammonia particle
356 formation scheme. There may be other significant mechanisms present, e.g. sulfuric acid - amine particle
357 formation (Bergman et al., 2015), with a geographical pattern resembling that of our results. Both
358 mechanisms depend on sulfuric acid concentration predictions, which may be inaccurate as well. We

359 compared the modeled and measured acid concentrations at one of the measurement sites (Melpitz), and
360 found that the modeled concentrations were slightly overpredicted (Fig. S2 in the supplement). This
361 may also contribute to the overprediction of the small particle sizes.

362

363 **3.2 Vertical profiles of particle number concentrations**

364 In this section we investigate the vertical distribution of the means of N_{tot} , N_{10} , N_{50} and N_{100} along with
365 parameters relevant for predicting NPF for the base case simulations (Fig. 3). These parameters include
366 gas-phase concentrations of H_2SO_4 , NH_3 , RH and T . In the results shown in Fig. 3 the TUV radiation
367 scheme has been used, thus representing the baseline simulation ACDC-TUV-DE. As can be seen from
368 Fig. 3, particles smaller than 10 nm contribute significantly to the total number concentration throughout
369 the tropospheric column, N_{tot} is about one order of magnitude greater than N_{10} and two and three orders
370 of magnitudes greater than N_{50} and N_{100} , respectively. Values of N_{10} , N_{50} and N_{100} decrease monotonically
371 with altitude, dropping significantly at approximately 1 km (layers 6-8 of the model). The vertical
372 distribution of N_{tot} shows a different trend at higher altitudes where a bump in N_{tot} occurs at around 6-
373 11 km, although no significant increase in the gas-phase concentration of H_2SO_4 and NH_3 are predicted
374 at these altitudes (Fig. 3). The increase in N_{tot} is mostly due to a significantly decreased coagulation sink
375 for the newly formed particles, as the number of larger particles dramatically decreases with altitude,
376 and partly due to the rapidly decreasing temperature. PMCAMx-UF predicts the particle formation rates
377 to decrease rapidly from around 2 km upward. The temperature, RH and sulfuric acid profile have
378 similar relative trends as the N_{10} , N_{50} and N_{100} profiles. There is a plateau in temperature and RH (at the
379 temperature range 285-288 K and RH range 80-83 %) profile up to altitude 1.2 km. Above this altitude,
380 however, the RH and temperature values decrease rapidly. The sharp decreases in the relative humidity,
381 temperature and particle number concentrations are consistent with the location of the boundary layer
382 height. This is in agreement with Ferrero et al., (2010) who showed that mixing height estimations (over
383 the city of Milan) derived from particle number concentration, temperature and relative humidity are
384 correlated with one another.

385 Figure 4 shows the comparison of the two simulations ACDC-TUV-DE and Napari-TUV-DE (see Table
386 1) with the observational data collected during the EUCAARI-LONGREX campaign measured by
387 German DLR Falcon 20 and the British FAAM BAe-146 aircraft. The overall statistics of the
388 comparisons between the modeled concentrations in all the simulations using the TUV radiation scheme
389 and the aircraft data are presented in Supplementary Table S2. The model using the ACDC-based
390 formation rates predicts the number concentration profile of particles larger than 4 nm (N_4) within about
391 one order of magnitude of the observed N_4 profile throughout the atmospheric column. The scaled
392 Napari NPF scheme leads to N_4 concentrations closer to the observations than those using the ACDC
393 scheme with biases less than 50 %. As mentioned above, the vertical profiles presented in Figure 4 are
394 produced by the model using the TUV radiation scheme. A similar analysis of the vertical profiles using

395 the RADM radiation scheme (simulation ACDC-RADM-DE), which is not shown here, results in
396 exactly the same shape of the number concentration profiles. The vertical profiles using the RADM
397 radiation scheme show minimal, yet worse, difference in the absolute number concentrations from the
398 observations compared to the TUV radiation scheme. The number concentrations of particles larger than
399 10 nm (N_{10}) predicted by the model using the scaled Napari NPF scheme agree well with the observations
400 throughout the atmospheric column (NMB less than 20 %, see Table S2). The model using the ACDC
401 formation rates tends to overpredict the N_{10} profile (NMB between 173-249 %). The shape of the
402 observed N_{10} vertical profile is captured throughout the atmospheric column regardless of the NPF
403 scheme used. Both model versions have almost the same performance for the $N_{160-1040}$ profile within the
404 boundary layer; both simulations (i.e. ACDC-TUV-DE and Napari-TUV-DE) underpredicting the N_{160-}
405 $_{1040}$ profile by about a factor of five. This behavior is seen in the $N_{160-1040}$ profile corresponding to both
406 observational data sets (i.e. Falcon 20, Fig. 4-d, and BAe 146, Fig 4-e aircraft data). This is at least partly
407 due to the lack of sources of organic condensable vapors to grow the particles to larger sizes in the model
408 (Patoulias et al., 2015), which will be investigated in a future study. The underprediction decreases for
409 all model versions at altitudes above the boundary layer improving the agreement with observational
410 data.

411 The results for the model using the ACDC-based formation rates are comparable to previous studies.
412 For example, Reddington et al. (2011) tested different NPF parameterizations in the BL including
413 activation, kinetic and combined organic- H_2SO_4 parameterizations, which are implemented in the
414 Global Model of Aerosol Processes (GLOMAP). The evaluation of the modeled vertical profiles of
415 particle number concentrations against the aircraft measurements showed that all of the mentioned NPF
416 schemes dramatically underpredicted particles in nucleation (normalized mean bias (NMB) varies from
417 -33 to -96) and Aitken-mode sizes ($-44 < NMB < -59$). The larger particles (N_{100}) however were
418 generally well-captured by the model. Furthermore, Lupascu et al. (2015) compared simulated number
419 concentrations with aircraft measurements collected during the Carbonaceous Aerosol and Radiative
420 Effects Study (CARES) campaign. They also tested different NPF parameterizations including
421 activation, kinetic and combined organic- H_2SO_4 parameterizations, which are implemented in the
422 regional-scale model WRF-Chem one-at-a-time using a sectional framework to simulate the NPF. They
423 found that their simulations overpredicted the particle number concentrations, especially in the smallest
424 sizes (normalized mean bias of 126-608 % for N_3 and N_{10}). The nucleation scheme had very little impact
425 on the magnitude of the CCN-sized particle number concentrations.

426

427 **3.3 Effect of the radiative-transfer scheme on predictions of particle number concentrations**

428 Updating the radiative-transfer scheme to the TUV scheme has a small effect on the predicted number
429 concentrations; the vertical profile of the relative difference $(N_{TUV} - N_{RADM}) \times 100 / N_{RADM}$ in the May-

430 2008 domain mean particle number concentrations shows a maximum reduction of about -5.5 % in N_{tot}
431 (at altitude 2.2 km) and a maximum increase of about 9 % in N_{100} (at altitude range 0.7-2.2 km). Figure
432 5 shows the spatial distribution of the absolute difference of the H_2SO_4 gas phase concentration and total
433 particle number concentrations between the simulations ACDC-TUV-DE and ACDC-RADM-DE (see
434 Table 1) at 12:00 UTC on May 5, 2008. Figure 5 also presents the cloud optical depth fields to illustrate
435 the link between the cloud fields and changes in the particle number concentrations due to the new cloud
436 adjustment scheme. The TUV scheme results in higher particle formation rates above and in the vicinity
437 of the cloudy regions due to enhanced radiation and sulfuric acid production. This is in agreement with
438 observations reported by Wehner et al. (2015). They concluded that the cloudy regions provide a
439 favorable environment for NPF above and at the edges of clouds due to enhanced upward spectral
440 irradiance and cloud-reflected spectral radiance around them. Sulfuric acid concentration is reduced
441 below cloud in the TUV scheme, due to the enhanced UV attenuation scaling down the photolysis rates.
442 However, as pointed out above, the effect on the total particle number concentrations is generally small.

443 **4 Conclusions**

444 We have updated the new particle formation (NPF) scheme within PMCAMx-UF with particle
445 formation rates for the ternary $\text{H}_2\text{SO}_4\text{-NH}_3\text{-H}_2\text{O}$ pathway simulated by the Atmospheric Cluster
446 Dynamics Code using quantum chemical input data. The ACDC results were implemented in
447 PMCAMx-UF as a lookup table from which the formation rates were interpolated. We believe this is
448 the first time that reasonable particle concentrations have been produced in a large-scale atmospheric
449 model with a NPF scheme without any scaling factors or location/condition dependent semi-empiricism.
450 In addition to the updated NPF description, we have also updated PMCAMx-UF treatment of the
451 cloudiness effect on the photolysis rates (i.e. cloud adjustment scheme) profile by implementing a
452 streamlined version of the Tropospheric Ultraviolet and Visible radiative-transfer model (Madronich,
453 2002).

454 We used the updated PMCAMx-UF to simulate particle number concentration during May 2008 over
455 Europe. During this period, the EUCAARI campaign was performed to measure the particle number
456 size distributions within the atmospheric boundary layer at various European Supersites for Atmospheric
457 Aerosol Research (EUSAAR) in addition to higher altitude data collected by two research aircraft during
458 the LONGREX campaign. Comparing the measured particle number concentrations at the EUSAAR
459 sites to the predictions of the updated PMCAMx-UF shows that the model slightly overpredicts
460 concentrations for particles with diameters between 10-100 nm. Particles larger than 100 nm are slightly
461 underpredicted. For details of the model performance statistics, the reader is referred to Supporting
462 Tables S1 and S2.

463 Vertical profiles of particle number concentrations show that predicted concentrations of small particles
464 are within one order of magnitude of the aircraft measurements. The predicted Aitken- and
465 accumulation-mode number concentrations are in quite good agreement with the observational data
466 throughout the atmospheric column, while the concentrations of smaller particles are somewhat
467 overpredicted by the ACDC-based NPF scheme. Including organic condensation onto the ultrafine
468 particles could improve these predictions.

469 **Acknowledgements**

470 We gratefully acknowledge Oona Kupiainen-Määttä for providing the ACDC-simulation data and
471 generating the look-up table. Tinja Olenius is acknowledged for discussions and technical support
472 related to ACDC, Radovan Krejci for providing the EUCAARI-LONGREX data, and Samuel Lowe for
473 comments on the language. The updated NPF and TUV modules are available from I. Riipinen
474 (ilona.riipinen@aces.su.se). Falcon measurements and data analysis were funded by EUCAARI
475 (European Integrated project on Aerosol Cloud Climate and Air Quality interactions) project No.
476 036833-2 and by DLR. The UK aircraft experiment was supported through EUCAARI and the UK
477 Natural Environment Research Council through the APPRAISE programme, grant NE/E01108X/1. The
478 authors also thank the Academy of Finland Center of Excellence program (project number 272041), the
479 Nordic Centre of Excellence CRAICC, Academy of Finland, ERC-StG-ATMOGAIN (278277) and
480 ERC-StG_MOCAPAF (257360).

481

482 **References**

- 483 Ahlm, L., Julin, J., Fountoukis, C., Pandis, S. N., and Riipinen, I.: Particle number concentrations over Europe in
484 2030: the role of emissions and new particle formation, *Atmos. Chem. Phys.*, 13, 10271-10283, doi:10.5194/acp-
485 13-10271-2013, 2013.
- 486 Adams, P. J., and Seinfeld, J. H, Predicting global aerosol size distributions in general circulation models, *J.*
487 *Geophys. Res.*, 107, 4370, doi:10.1029/2001JD001010, 2002.
- 488
- 489 Almeida, J., Schobesberger, S., Kürten, A., Ortega, I. K., Kupiainen-Määttä, O., Praplan, A. P., Adamov, A.,
490 Amorim, A., Bianchi, F., Breitenlechner, M., David, A., Dommen, J., Donahue, N. M., Downard, A., Dunne, E.,
491 Duplissy, J., Ehrhart, S., Flagan, R. C., Franchin, A., Guida, R., Hakala, J., Hansel, A., Heinritzi, M., Henschel,
492 H., Jokinen, T., Junninen, H., Kajos, M., Kangasluoma, J., Keskinen, H., Kupc, A., Kurtén, T., Kvashin, A. N.,
493 Laaksonen, A., Lehtipalo, K., Leiminger, M., Leppä, J., Loukonen, V., Makhmutov, V., Mathot, S., McGrath, M.
494 J., Nieminen, T., Olenius, T., Onnela, A., Petäjä, T., Riccobono, F., Riipinen, I., Rissanen, M., Rondo, L.,
495 Ruuskanen, T., Santos, F. D., Sarnela, N., Schallhart, S., Schnitzhofer, R., Seinfeld, J. H., Simon, M., Sipilä, M.,
496 Stozhkov, Y., Stratmann, F., Tomé, A., Tröstl, J., Tsagkogeorgas, G., Vaattovaara, P., Viisanen, Y., Virtanen, A.,
497 Vrtala, A., Wagner, P. E., Weingartner, E., Wex, H., Williamson, C., Wimmer, D., Ye, P., Yli-Juuti, T., Carslaw,
498 K. S., Kulmala, M., Curtius, J., Baltensperger, U., Worsnop, D. R., Vehkamäki, H., and Kirkby, J: Molecular
499 understanding of sulphuric acid-amine particle nucleation in the atmosphere. *Nature*, 502: 359-363,
500 doi:10.1038/nature12663, 2013.

501
502 Asmi, A., Wiedensohler, A., Laj, P., Fjaeraa, A.-M., Sellegri, K., Birmili, W., Weingartner, E., Baltensperger, U.,
503 Zdimal, V., Zikova, N., Putaud, J.-P., Marinoni, A., Tunved, P., Hansson, H.-C., Fiebig, M., Kivekäs, N.,
504 Lihavainen, H., Asmi, E., Ulevicius, V., Aalto, P. P., Swietlicki, E., Kristensson, A., Mihalopoulos, N., Kalivitis,
505 N., Kalapov, I., Kiss, G., de Leeuw, G., Henzing, B., Harrison, R. M., Beddows, D., O'Dowd, C., Jennings, S. G.,
506 Flentje, H., Weinhold, K., Meinhardt, F., Ries, L., and Kulmala, M.: Number size distributions and seasonality of
507 submicron particles in Europe 2008–2009, *Atmos. Chem. Phys.*, 11, 5505–5538, doi:10.5194/acp-11-5505-2011,
508 2011.
509
510 Bergman, T., Laaksonen, A., Korhonen, H., Malila, J., Dunne, E. M., Mielonen, T., Lehtinen, K. E. J., Kühn, T.,
511 Arola, A., and Kokkola, H.: Geographical and Diurnal Features of Amine-Enhanced Boundary Layer Nucleation
512 *J. Geophys. Res. Atmos.*, 120, 9606–9624, 2015.
513
514 Carslaw, K. S., Lee, L. A., Reddington, C. L., Pringle, K. J., Rap, A., Forster, P. M., Mann, G. W., Spracklen, D.
515 V., Woodhouse, M. T., Regayre, L. A., Pierce, J. R.: Large contribution of natural aerosols to uncertainty in indirect
516 forcing, *Nature* 503, 67–71, doi:10.1038/nature12674, 2013.
517
518 Chang, J. S., Brost, R. A., Isaksen, I. S. A., Madronich, S., Middleton, P., Stockwell, W. R., and Walcek, C. J.:
519 A three-dimensional Eulerian acid deposition model: Physical concepts and formulation, *J. Geophys.*
520 *Res.*, 92(D12), 14681–14700, doi:10.1029/JD092iD12p14681, 1987.
521
522 Cui, Z., Gadian, A., Blyth, A., Crosier, J., and Crawford, I.: Observations of the Variation in Aerosol and Cloud
523 Microphysics along the 20°S Transect on 13 November 2008 during VOCALS-Rex, *J. Atmos. Sci.*, 71, 2927–
524 2943, doi: <http://dx.doi.org/10.1175/JAS-D-13-0245.1>, 2014.
525
526 Dal Maso, M., Kulmala, M., Lehtinen, K. E. J., Mäkelä, J. M., Aalto, P., and O'Dowd, C. D.: Condensation and
527 coagulation sinks and formation of nucleation mode particles in coastal and boreal forest boundary layers, *J.*
528 *Geophys. Res.*, 107(D19), doi:10.1029/2001JD001053, 2002.
529
530 Denier van der Gon, H. A. C., Visschedijk, A. J. H., Johansson, C., Hedberg Larsson, E., Harrison, R., and
531 Beddows, D.: Size resolved pan European anthropogenic particle number inventory, EUCAARI Deliverable report
532 D141 (available on request from EUCAARI project office), 2009.
533
534 Emery, C., J. Jung, J. Johnson, G. Yarwood, and D. Boyer: Improving cloud impacts on photolysis using an on-
535 line radiation model in CAMx, presented at the 9th Annual CMAS Conference, pp. 9–14, 2010.
536
537 Ferrero, L., Perrone, M. G., Petraccone, S., Sangiorgi, G., Ferrini, B. S., Lo Porto, C., Lazzati, Z., Cocchi, D.,
538 Bruno, F., Greco, F., Riccio, A., and Bolzacchini, E.: Vertically-resolved particle size distribution within and above
539 the mixing layer over the Milan metropolitan area, *Atmos. Chem. Phys.*, 10, 3915–3932, doi:10.5194/acp-10-3915-
540 2010, 2010.
541
542 Fahey K. M., and Pandis, S. N.: Optimizing model performance: Variable size resolution in cloud chemistry
543 modeling, *Atmos. Environ.*, 35, 4471–4478, doi:10.1016/S1352-2310(01)00224-2, 2001.
544
545 Feldpausch, P., Fiebig, M., Fritzsche, L., and Petzold, A.: Measurement of ultrafine aerosol size distributions by a
546 combination of diffusion screen separators and condensation particle counters, *J. Aerosol Sci.*, 37, 577–597,
547 doi:10.1016/j.jaerosci.2005.04.009, 2006.
548
549 Fiebig, M., Stein, C., Schroder, F., Feldpausch, P., and Petzold, A.: Inversion of data containing information on the
550 aerosol particle size distribution using multiple instruments, *J. Aerosol Sci.*, 36, 1353–1372,
551 doi:10.1016/j.jaerosci.2005.01.004, 2005.
552

553 Fountoukis, C., Racherla, P. N., Denier van der Gon, H. A. C., Polymeneas, P., Charalampidis, P. E., Pilinis, C.,
554 Wiedensohler, A., Dall'Osto, M., O'Dowd, C., and Pandis, S. N.: Evaluation of a three-dimensional chemical
555 transport model (PMCAMx) in the European domain during the EUCAARI May 2008 campaign, *Atmos. Chem.*
556 *Phys.*, 11, 10331-10347, doi:10.5194/acp-11-10331-2011, 2011.

557

558 Fountoukis, C., Riipinen, I., Denier van der Gon, H. A. C., Charalampidis, P. E., Pilinis, C., Wiedensohler, A.,
559 O'Dowd, C., Putaud, J. P., Moerman, M., and Pandis, S. N.: Simulating ultrafine particle formation in Europe
560 using a regional CTM: contribution of primary emissions versus secondary formation to aerosol number
561 concentrations, *Atmos. Chem. Phys.*, 12, 8663-8677, doi:10.5194/acp-12-8663-2012, 2012.

562

563 Fuzzi, S., Baltensperger, U., Carslaw, K., Decesari, S., Denier van der Gon, H., Facchini, M. C., Fowler, D.,
564 Koren, I., Langford, B., Lohmann, U., Nemitz, E., Pandis, S., Riipinen, I., Rudich, Y., Schaap, M., Slowik, J. G.,
565 Spracklen, D. V., Vignati, E., Wild, M., Williams, M., and Gilardoni, S.: Particulate matter, air quality and climate:
566 lessons learned and future needs, *Atmos. Chem. Phys.*, 15, 8217-8299, doi:10.5194/acp-15-8217-2015, 2015.

567

568 Gaydos, T. M., Stanier, C. O., and Pandis, S. N.: Modelling of in situ ultrafine atmospheric particle formation in
569 the eastern United States, *J. Geophys. Res.*, 110, D07S12, doi:10.1029/2004JD004683, 2005.

570

571 Gaydos, T., Pinder, R., Koo, B., Fahey, K., Yarwood, G., and Pandis, S. N.: Development and application of a
572 three-dimensional aerosol chemical transport model, PMCAMx, *Atmos. Environ.*, 41, 2594-2611,
573 doi:10.1016/j.atmosenv.2006.11.034, 2007.

574

575 Guenther, A., Karl, T., Harley, P., Wiedinmyer, C., Palmer, P. I., and Geron, C.: Estimates of global terrestrial
576 isoprene emissions using MEGAN (Model of Emissions of Gases and Aerosols from Nature), *Atmos. Chem.*
Phys., 6, 3181-3210, doi:10.5194/acp-6-3181-2006, 2006.

577

578 Hamburger, T., McMeeking, G., Minikin, A., Birmili, W., Dall'Osto, M., O'Dowd, C., Flentje, H., Henzing, B.,
579 Junninen, H., Kristensson, A., de Leeuw, G., Stohl, A., Burkhardt, J. F., Coe, H., Krejci, R., and Petzold, A.:
580 Overview of the synoptic and pollution situation over Europe during the EUCAARI-LONGREX field campaign,
581 *Atmos. Chem. Phys.*, 11, 1065-1082, doi:10.5194/acp-11-1065-2011, 2011.

582

583 Hamburger, T., McMeeking, G., Minikin, A., Petzold, A., Coe, H., and Krejci, R.: Airborne observations of aerosol
584 microphysical properties and particle ageing processes in the troposphere above Europe, *Atmos. Chem. Phys.*, 12,
585 11533-11554, doi:10.5194/acp-12-11533-2012, 2012.

586

587 Henschel, H., Navarro, J. C. A., Yli-Juuti, T., Kupiainen-Määttä, O., Olenius, T., Ortega, I. K., Clegg, S. L.,
588 Kurtén, T., Riipinen, I., and Vehkamäki, H.: Hydration of atmospherically relevant molecular clusters:
589 Computational chemistry and classical thermodynamics. *J. Phys. Chem. A.*, 118: 2599-2611,
590 doi:10.1021/jp500712y, 2014.

591

592 Henschel, H., Kurtén, T., and Vehkamäki, H.: A computational study on the effect of hydration on new particle
593 formation in the sulfuric acid/ammonia and sulfuric acid/dimethylamine systems, submitted to *Journal of Physical*
594 *Chemistry*, 2015

595

596 Jen, C. N., P. H. McMurry, and D. R. Hanson: Stabilization of sulfuric acid dimers by ammonia, methylamine,
597 dimethylamine, and trimethylamine, *J. Geophys. Res.*, 119, 7502-7514, doi:10.1002/2014JD021592, 2014.

598

599 Jung, J., Adams, P. J., and Pandis, S. N.: Simulating the size distribution and chemical composition of ultrafine
600 particles during nucleation events, *Atmospheric Environment*, 40(13), 2248-2259, doi:10.1016/j.atmosenv.2005.09.082, 2006.

601

602 Jung, J. G., Pandis, S. N., and Adams, P. J.: Evaluation of nucleation theories in a sulfur-rich environment. *Aerosol*
603 *Sci. Technol.*, 42(7), 495-504, doi:10.1080/02786820802187085, 2008.

604
605 Jung, J., Fountoukis, C., Adams, P. J., and Pandis, S. N.: Simulation of in situ ultrafine particle formation in the
606 eastern United States using PMCAMx-UF, *J. Geophys. Res.*, 115, D03203, doi:10.1029/2009JD012313, 2010.
607
608 Karydis, V. A., Tsimpidi, A. P., and Pandis, S. N.: Evaluation of a three-dimensional chemical transport model
609 (PMCAMx) in the eastern United States for all four seasons, *J. Geophys. Res.*, 112, D14211,
610 doi:10.1029/2006JD007890, 2007.
611
612 Kerminen, V.-M., Paramonov, M., Anttila, T., Riipinen, I., Fountoukis, C., Korhonen, H., Asmi, E., Laakso, L.,
613 Lihavainen, H., Swietlicki, E., Svenningsson, B., Asmi, A., Pandis, S. N., Kulmala, M., and Petäjä, T.: Cloud
614 condensation nuclei production associated with atmospheric nucleation: a synthesis based on existing literature
615 and new results, *Atmos. Chem. Phys.*, 12, 12037-12059, doi:10.5194/acp-12-12037-2012, 2012.
616
617 Kirkby, J., Duplissy, J., Sengupta, K., Frege, C., Gordon, H., Williamson, C., Heinritzi, M., Simon, M., Yan, C.,
618 Almeida, J., Tröstl, J., Nieminen, T., Ortega, I. K., Wagner, R., Adamov, A., Amorim, A., Bernhammer, A.,
619 Bianchi, F., Breitenlechner, M., Brilke, S., Chen, X., Craven, J., Dias, A., Ehrhart, S., Flagan, R. C., Franchin, A.,
620 Fuchs, C., Guida, R., Hakala, J., Hoyle, C. R., Jokinen, T., Junninen, H., Kangasluoma, J., Kim, J., Krapf, M.,
621 Kürten, A., Laaksonen, A., Lehtipalo, K., Makhmutov, V., Mathot, S., Molteni, U., Onnela, A., Peräkylä, O., Piel,
622 F., Petäjä, T., Praplan, A. P., Pringle, K., Rap, A., Richards, N. A. D., Riipinen, I., Rissanen, M. P., Rondo, L.,
623 Sarnela, N., Schobesberger, S., Scott, C. E., Seinfeld, J. H., Sipilä, M., Steiner, G., Stozhkov, Y., Stratmann, F.,
624 Tomé, A., Virtanen, A., Vogel, A. L., Wagner, A. C., Wagner, P. E., Weingartner, E., Wimmer, D., Winkler, P.
625 M., Ye, P., Zhang, X., Hansel, A., Dommen, J., Donahue, N. M., Worsnop, D. R., Baltensperger, U., Kulmala, M.,
626 Carslaw, K. S., Curtius, J.: Ion-induced nucleation of pure biogenic particles, *Nature* 533, 521-526,
627 doi:10.1038/nature17953, 2016.
628
629 Kirkby, J., Curtius, J., Almeida, J., Dunne, E., Duplissy, J., Ehrhart, S., Franchin, A., Gagné, S., Ickes, L., Kürten,
630 A., Kupc, A., Metzger, A., Riccobono, F., Rondo, L., Schobesberger, S., Tsagkogeorgas, G., Wimmer, D.,
631 Amorim, A., Bianchi, F., and Breitenlechner, M.: Role of sulphuric acid, ammonia and galactic cosmic rays in
632 atmospheric aerosol nucleation, *Nature* 476, 429-433, doi:10.1038/nature10343, 2011.
633
634 Korhonen, P., Kulmala, M., Laaksonen, A., Viisanen, Y., McGraw, R. and Seinfeld, J. H.: Ternary nucleation of
635 H₂SO₄, NH₃, and H₂O in the atmosphere, *J. Geophys. Res.*, 104, 26349–26353, doi:10.1029/1999JD900784, 1999.
636
637 Kulmala, M., Liisa, P, and Mäkelä, J. M.: Stable sulphate clusters as a source of new atmospheric
638 particles, *Nature* 404, no. 6773, 66-69, doi: 10.1038/35003550, 2000.
639
640 Kulmala, M., Vehkamäki, H., Petäjä, T., Dal Maso, M., Lauri, A., Kerminen, V.-M., Birmili, and W., McMurry,
641 P.H.: Formation and growth rates of ultrafine atmospheric particles: a review of observations, *J Aerosol Sci.*,
642 35:143-76, doi:10.1016/j.jaerosci.2003.10.003, 2004.
643
644 Kulmala, M., Lehtinen, K. E. J., and Laaksonen, A.: Cluster activation theory as an explanation of the linear
645 dependence between formation rate of 3 nm particles and sulphuric acid concentration, *Atmos. Chem. Phys.*, 6,
646 787–793, doi:10.5194/acp-6-787-2006, 2006.
647
648 Kulmala, M., Asmi, A., Lappalainen, H. K., Carslaw, K. S., Pöschl, U., Baltensperger, U., Hov, Ø., Brenquier, J.-
649 L., Pandis, S. N., Facchini, M. C., Hansson, H.-C., Wiedensohler, A., and O'Dowd, C. D.: Introduction: European
650 Integrated Project on Aerosol Cloud Climate and Air Quality interactions (EUCAARI) – integrating aerosol
651 research from nano to global scales, *Atmos. Chem. Phys.*, 9, 2825-2841, doi:10.5194/acp-9-2825-2009, 2009.

652 Kulmala, M., Asmi, A., Lappalainen, H. K., Baltensperger, U., Brenguier, J.-L., Facchini, M. C., Hansson, H.-C.,
653 Hov, Ø., O'Dowd, C. D., Pöschl, U., Wiedensohler, A., Boers, R., Boucher, O., de Leeuw, G.,
654 Denier van der Gon, H. A. C., Feichter, J., Krejci, R., Laj, P., Lihavainen, H., Lohmann, U., McFiggans, G.,
655 Mentel, T., Pilinis, C., Riipinen, I., Schulz, M., Stohl, A., Swietlicki, E., Vignati, E., Alves, C., Amann, M.,
656 Ammann, M., Arabas, S., Artaxo, P., Baars, H., Beddows, D. C. S., Bergström, R., Beukes, J. P., Bilde, M.,
657 Burkhart, J. F., Canonaco, F., Clegg, S. L., Coe, H., Crumeyrolle, S., D'Anna, B., Decesari, S., Gilardoni, S.,
658 Fischer, M., Fjaeraa, A. M., Fountoukis, C., George, C., Gomes, L., Halloran, P., Hamburger, T., Harrison, R. M.,
659 Herrmann, H., Hoffmann, T., Hoose, C., Hu, M., Hyvärinen, A., Hörrak, U., Iinuma, Y., Iversen, T., Josipovic, M.,
660 Kanakidou, M., Kiendler-Scharr, A., Kirkevåg, A., Kiss, G., Klimont, Z., Kolmonen, P., Komppula, M.,
661 Kristjánsson, J.-E., Laakso, L., Laaksonen, A., Labonnote, L., Lanz, V. A., Lehtinen, K. E. J., Rizzo, L. V.,
662 Makkonen, R., Manninen, H. E., McMeeking, G., Merikanto, J., Minikin, A., Mirme, S., Morgan, W. T.,
663 Nemitz, E., O'Donnell, D., Panwar, T. S., Pawlowska, H., Petzold, A., Pienaar, J. J., Pio, C., Plass-Duelmer, C.,
664 Prévôt, A. S. H., Pryor, S., Reddington, C. L., Roberts, G., Rosenfeld, D., Schwarz, J., Seland, Ø., Sellegri, K.,
665 Shen, X. J., Shiraiwa, M., Siebert, H., Sierau, B., Simpson, D., Sun, J. Y., Topping, D., Tunved, P., Vaattovaara, P.,
666 Vakkari, V., Veeffkind, J. P., Visschedijk, A., Vuollekoski, H., Vuolo, R., Wehner, B., Wildt, J., Woodward, S.,
667 Worsnop, D. R., van Zadelhoff, G.-J., Zardini, A. A., Zhang, K., van Zyl, P. G., Kerminen, V.-M., Carslaw, K.,
668 and Pandis, S. N.: General overview: European Integrated project on Aerosol Cloud Climate and Air Quality
669 interactions (EUCAARI) – integrating aerosol research from nano to global scales, *Atmos. Chem. Phys.*, 11,
670 13061-13143, doi:10.5194/acp-11-13061-2011, 2011.

671
672 Laaksonen, A., Kulmala, M., Berndt, T., Stratmann, F., Mikkonen, S., Ruuskanen, A., Lehtinen, K. E. J.,
673 Dal Maso, M., Aalto, P., Petäjä, T., Riipinen, I., Sihto, S.-L., Janson, R., Arnold, F., Hanke, M., Ücker, J.,
674 Umann, B., Sellegri, K., O'Dowd, C. D., and Viisanen, Y.: SO₂oxidation products other than H₂SO₄ as a trigger of
675 new particle formation. Part 2: Comparison of ambient and laboratory measurements, and atmospheric
676 implications, *Atmos. Chem. Phys.*, 8, 7255-7264, doi:10.5194/acp-8-7255-2008, 2008.

677
678 Liu, P. S. K., Leitch, W. R., Strapp, J. W., and Wasey, M. A.: Response of Particle Measuring Systems Airborne
679 ASASP and PCASP to NaCl and Latex Particles, *Aerosol Sci. Technol.*, 16, 83-95,
680 doi:0.1080/02786829208959539, 1992.

681
682 Lupascu, A., Easter, R., Zaveri, R., Shrivastava, M., Pekour, M., Tomlinson, J., Yang, Q., Matsui, H., Hodzic, A.,
683 Zhang, Q., and Fast, J. D.: Modeling particle nucleation and growth over northern California during the 2010
684 CARES campaign, *Atmos. Chem. Phys. Discuss.*, 15, 19729-19801, doi:10.5194/acpd-15-19729-2015, 2015.

685
686 Madronich, S., National Center for Atmospheric Research, Boulder, Colorado, (2002). Tropospheric ultraviolet
687 and visible radiation model. [Available online at <http://acd.ucar.edu/models/UV/TUV/index.html>.]

688
689 Makkonen, R., Asmi, A., Korhonen, H., Kokkola, H., Järvenoja, S., Räisänen, P., Lehtinen, K. E. J., Laaksonen, A.,
690 Kerminen, V.-M., Järvinen, H., Lohmann, U., Bennartz, R., Feichter, J., and Kulmala, M.: Sensitivity of aerosol
691 concentrations and cloud properties to nucleation and secondary organic distribution in ECHAM5-HAM global
692 circulation model, *Atmos. Chem. Phys.*, 9, 1747-1766, doi:10.5194/acp-9-1747-2009, 2009.

693
694 Matsui, H., M. Koike, Y. Kondo, N. Takegawa, A. Wiedensohler, J. D. Fast, and R. A. Zaveri: Impact of new
695 particle formation on the concentrations of aerosols and cloud condensation nuclei around Beijing, *J. Geophys.*
696 *Res.*, 116, D19208, doi:10.1029/2011JD016025, 2011.

697
698 Matsui, H., M. Koike, N. Takegawa, Y. Kondo, A. Takami, T. Takamura, S. Yoon, S.-W. Kim, H.-C. Lim, and J.
699 D. Fast: Spatial and temporal variations of new particle formation in East Asia using an NPF-explicit WRF-chem
700 model: North-south contrast in new particle formation frequency, *J. Geophys. Res. Atmos.*, 118, 11,647–11,663,
701 doi:10.1002/jgrd.50821, 2013.

702
703 McMurry, P.: Photochemical aerosol formation from SO₂: A theoretical analysis of smog chamber data, *J. Colloid*
704 *Interface Sci.*, 78(2), 513–527, doi:10.1016/0021-9797(80)90589-5, 1980.

705
706 Merikanto, J., Spracklen, D. V., Mann, G. W., Pickering, S. J., and Carslaw, K. S.: Impact of nucleation on global
707 CCN, *Atmos. Chem. Phys.*, 9, 8601–8616, doi:10.5194/acp-9-8601-2009, 2009.
708
709 Merikanto J., Zupadinsky E., Lauri A., Vehkamäki H.: Origin of the Failure of Classical Nucleation Theory:
710 Incorrect Description of the Smallest Clusters, *Phys. Rev. Lett.*, 98, 145702, doi:10.1103/PhysRevLett.98.145702,
711 2007a.
712
713 Merikanto, J., Napari, I., Vehkamäki, H., Anttila, T., and Kulmala, M.: New parameterization of sulfuric acid-
714 ammonia-water ternary nucleation rates at tropospheric conditions, *J. Geophys. Res.*, 112, D15207,
715 doi:10.1029/2006JD007977, 2007b.
716
717 Napari, I., Kulmala, M., and Vehkamäki, H.: Ternary nucleation of inorganic acids, ammonia, and water, *J. Chem.*
718 *Phys.*, 117, 8418–8425, doi:10.1063/1.1511722, 2002.
719
720 O'Dowd, C. D., B. Langmann, S. Varghese, C. Scannell, D. Ceburnis, and M. C. Facchini: A combined organic-
721 inorganic sea-spray source function, *Geophys. Res. Lett.*, 35, L01801, doi:10.1029/2007GL030331, 2008.
722
723 Olenius, T., Kupiainen-Määttä, O., Ortega, I. K., Kurtén, T., and Vehkamäki, H.: Free energy barrier in the growth
724 of sulfuric acid–ammonia and sulfuric acid–dimethylamine clusters, *J. Chem. Phys.*, 139: 084312,
725 doi:10.1063/1.4819024, 2013.
726
727 Ortega, I. K., Kupiainen, O., Kurtén, T., Olenius, T., Wilkman, O., McGrath, M. J., Loukonen, V., and
728 Vehkamäki, H.: From quantum chemical formation free energies to evaporation rates, *Atmos. Chem. Phys.*, 12,
729 225–235, doi:10.5194/acp-12-225-2012, 2012.
730
731 Paasonen, P., Nieminen, T., Asmi, E., Manninen, H. E., Petäjä, T., Plass-Dülmer, C., Flentje, H., Birmili, W.,
732 Wiedensohler, A., Hörrak, U., Metzger, A., Hamed, A., Laaksonen, A., Facchini, M. C., Kerminen, V.-M., and
733 Kulmala, M.: On the roles of sulphuric acid and low-volatility organic vapours in the initial steps of atmospheric
734 new particle formation, *Atmos. Chem. Phys.*, 10, 11223–11242, doi:10.5194/acp-10-11223-2010, 2010.
735
736 Patoulias, D., Fountoukis, C., Riipinen, I., and Pandis, S. N.: The role of organic condensation on ultrafine particle
737 growth during nucleation events, *Atmos. Chem. Phys.*, 15, 6337–6350, doi:10.5194/acp-15-6337-2015, 2015.
738
739 Pierce, J. R. and Adams, P. J.: A computationally efficient aerosol nucleation/ condensation method:
740 pseudo-steady-state sulfuric acid, *aerosol science and technology*, 43:3, 216–226, doi:
741 10.1080/02786820802587896, 2009.
742
743 Reddington, C. L., Carslaw, K. S., Spracklen, D. V., Frontoso, M. G., Collins, L., Merikanto, J., Minikin, A.,
744 Hamburger, T., Coe, H., Kulmala, M., Aalto, P., Flentje, H., Plass-Dülmer, C., Birmili, W., Wiedensohler, A.,
745 Wehner, B., Tuch, T., Sonntag, A., O'Dowd, C. D., Jennings, S. G., Dupuy, R., Baltensperger, U., Weingartner, E.,
746 Hansson, H.-C., Tunved, P., Laj, P., Sellegri, K., Boulon, J., Putaud, J.-P., Gruening, C., Swietlicki, E., Roldin, P.,
747 Henzing, J. S., Moerman, M., Mihalopoulos, N., Kouvarakis, G., Ždímal, V., Zíková, N., Marinoni, A.,
748 Bonasoni, P., and Duchi, R.: Primary versus secondary contributions to particle number concentrations in the
749 European boundary layer, *Atmos. Chem. Phys.*, 11, 12007–12036, doi:10.5194/acp-11-12007-2011, 2011.
750
751 Sihto, S.-L., Kulmala, M., Kerminen, V.-M., Dal Maso, M., Petäjä, T., Riipinen, I., Korhonen, H., Arnold, F.,
752 Janson, R., Boy, M., Laaksonen, A., and Lehtinen, K. E. J.: Atmospheric sulphuric acid and aerosol formation:
753 implications from atmospheric measurements for nucleation and early growth mechanisms, *Atmos. Chem. Phys.*,
754 6, 4079–4091, doi:10.5194/acp-6-4079-2006, 2006.
755
756 Skamarock, W. C., Klemp, J. B., Dudhia, J., Gill, D. O. Barker, D. M., and Wang, W.: A Description of the
757 Advanced Research WRF Version 2, NCAR Technical Note

758 (<http://opensky.ucar.edu/islandora/object/technotes%3A479/datastream/PDF/view>), doi:10.5065/D6DZ069T,
759 2005.
760
761 Sofiev, M., Vankevich, R., Lanne, M., Koskinen, J., and Kukkonen, J.: On integration of a Fire Assimilation System
762 and a chemical transport model for near-real-time monitoring of the impact of wild-land fires on atmospheric
763 composition and air quality, *Modelling, Monitoring and Management of Forest Fires*, WIT Transactions on
764 Ecology and the Environment, 119, 343–351, 2008a.
765
766 Sofiev, M., Lanne, M., Vankevich, R., Prank, M., Karppinen, A., and Kukkonen, J.: Impact of wild-land fires on
767 European air quality in 2006–2008, *Modelling, Monitoring and Management of Forest Fires*, WIT Transactions
768 on Ecology and the Environment, 119, 353–361, 2008b.
769
770 Spracklen, D. V., Carslaw, K. S., Kulmala, M., Kerminen, V.-M., Mann, G. W., and Sihto, S.-L.: The contribution
771 of boundary layer nucleation events to total particle concentrations on regional and global scales, *Atmos. Chem.*
772 *Phys.*, 6, 5631–5648, doi:10.5194/acp-6-5631-2006, 2006.
773
774 Takemura, T., Nakajima, O., Dubovik, B.N., Holben, S., Kinne: Single scattering albedo and radiative forcing of
775 various aerosol species with a global threedimensional model. *J. Climate*, 15, 3333–3352, doi:10.1175/1520-
776 0442(2002)015<0333:SSAARF>2.0.CO;2, 2002.
777
778 Vehkamäki, H., Kulmala, M., Napari, I., Lehtinen, K. E. J., Timmreck, C., Noppel, M., and Laaksonen, A.: An
779 improved parameterization for sulfuric acid-water nucleation rates for tropospheric and stratospheric conditions,
780 *J. Geophys. Res.*, 107, 4622, doi:10.1029/2002JD002184, 2002.
781
782 Visschedijk, A. J. H., Zandveld, P., and Denier van der Gon, H. A. C.: TNO Report 2007 A R0233/B: A high
783 resolution gridded European emission database for the EU integrated project GEMS, Netherlands, Organization
784 for Applied Scientific Research, 2007.
785
786 Westervelt, D. M., Pierce, J. R., and Adams, P. J.: Analysis of feedbacks between nucleation rate, survival
787 probability and cloud condensation nuclei formation, *Atmos. Chem. Phys.*, 14, 5577–5597, doi:10.5194/acp-14-
788 5577-2014, 2014.
789
790 Yu, F.: Effect of ammonia on new particle formation: A kinetic $\text{H}_2\text{SO}_4\text{-H}_2\text{O-NH}_3$ nucleation model constrained by
791 laboratory measurements, *J. Geophys. Res.*, 111, D01204, doi:10.1029/2005JD005968, 2006a.
792
793 Yu, F., and Luo, G.: Simulation of particle size distribution with a global aerosol model: contribution of nucleation
794 to aerosol and CCN number concentrations, *Atmos. Chem. Phys.*, 9, 7691–7710, doi:10.5194/acp-9-7691-2009,
795 2009.
796
797 Yu, F., Luo, G., Bates, T. S., Anderson, B., Clarke, A., Kapustin, V., Yantosca, R. M., Wang, Y., and WU, S.:
798 Spatial distributions of particle number concentrations in the global troposphere: Simulations, observations, and
799 implications for nucleation mechanisms, *J. Geophys. Res.*, 115, D17205, doi:10.1029/2009JD013473, 2010.
800
801 Zhang, Y., McMurry, P. H., Yu, F., and Jacobson, M. Z.: A comparative study of nucleation parameterizations: 1.
802 Examination and evaluation of the formulations, *J. Geophys. Res.*, 115, D20212, doi:10.1029/2010JD014150,
803 2010.
804
805
806
807
808

809

810

811 **Figures and figure captions**

812 Table 1. Summary of PMCAMx-UF model simulations reported in this study. The arithmetic mean of
 813 ground-level number concentration during May 2008 for particles larger than 0.8 nm (N_{tot}), 50 nm (N_{50})
 814 and 100 nm (N_{100}) is given for each simulation.

Simulation name	NPF scheme	Cloud adjustment scheme	Emissions	Domain mean number concentration (cm^{-3})		
				N_{tot}	N_{50}	N_{100}
ACDC-TUV-DE*	ACDC-based	TUV	Default	59200	1300	360
ACDC-RADM-DE	ACDC-based	RADM	Default	62000	1200	340
ACDC-TUV-NE*	ACDC-based	TUV	Updated	48300	1300	380
Napari-TUV-DE	Scaled Napari et al., 2002	TUV	Default	8100	1500	410
Napari-RADM-DE	Scaled Napari et al., 2002	RADM	Default	9000	1500	400

815 * DE = default emissions. The “default emissions” refer to the emissions used in Fountoukis et al.,
 816 2012 (simulation Napari-RADM-DE).

817 * NE = new emissions, including natural emissions from biogenic, marine and wildfire sources.

818

819

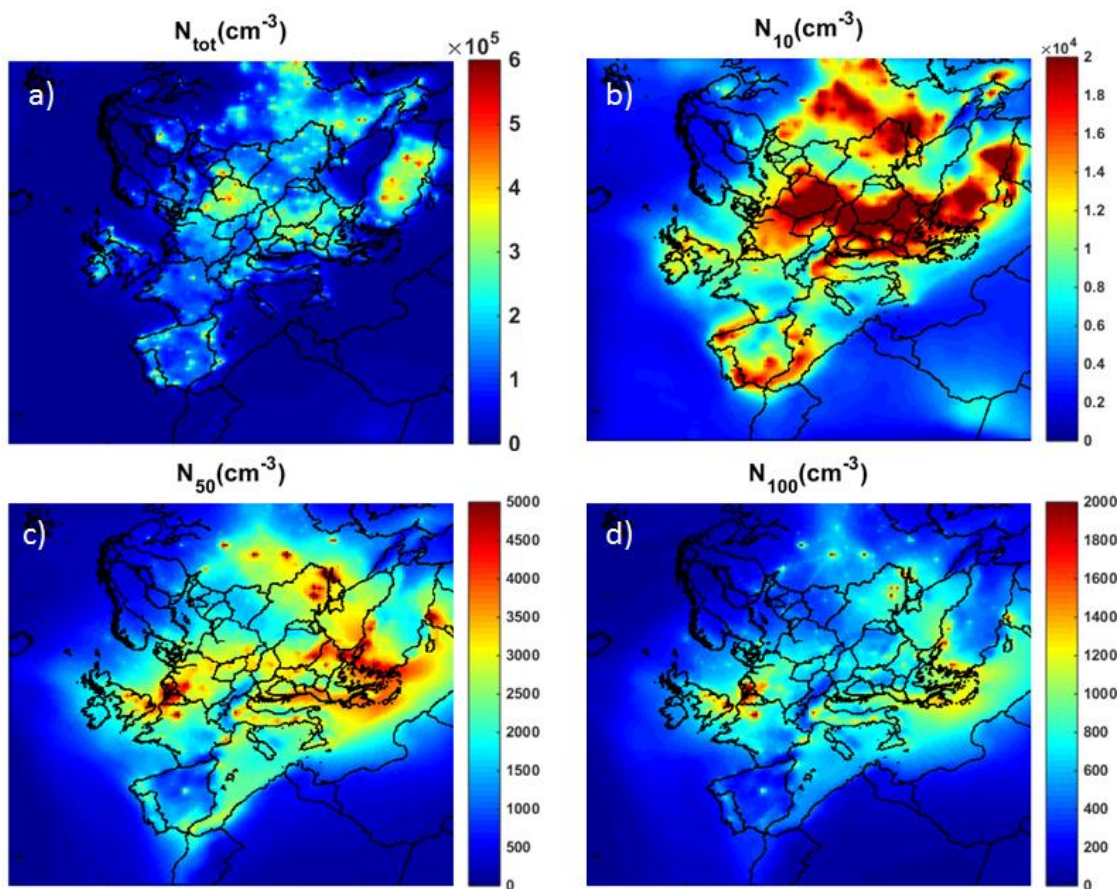
820

821

822

823

824



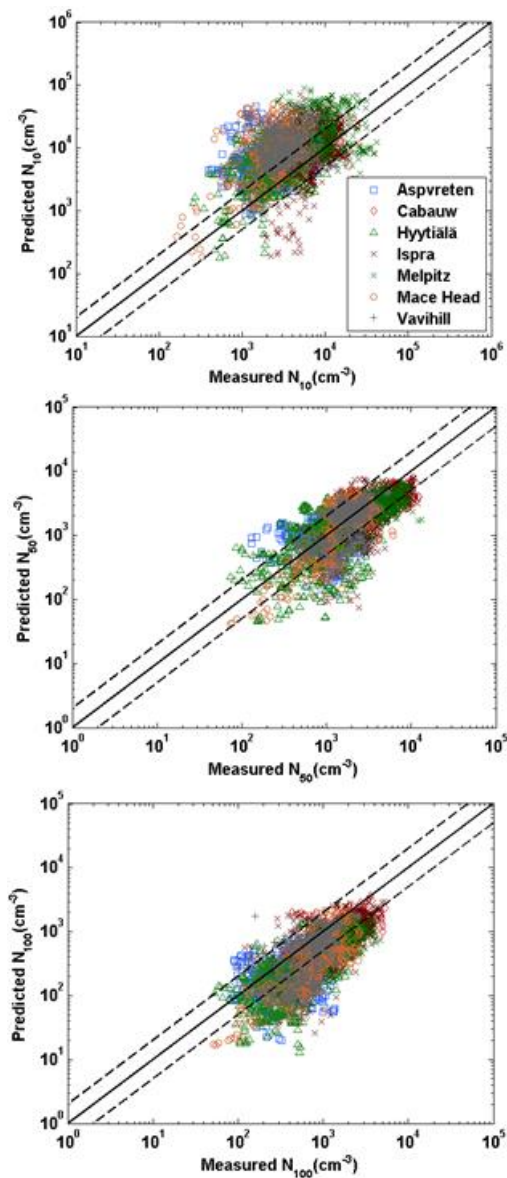
826

827 Figure 1. The simulated spatial distribution of the arithmetic mean of ground-level number concentration
 828 during May 2008 for particles larger than (a) 0.8 nm (N_{tot}), (b) 10 nm (N_{10}), (c) 50 nm (N_{50}), and (d)
 829 nm (N_{100}). The PMCAMx-UF baseline simulation ACDC-TUV-DE is used (see Table 1). Note that
 830 different color bar scales are used for the different size ranges for readability.

831

832

833



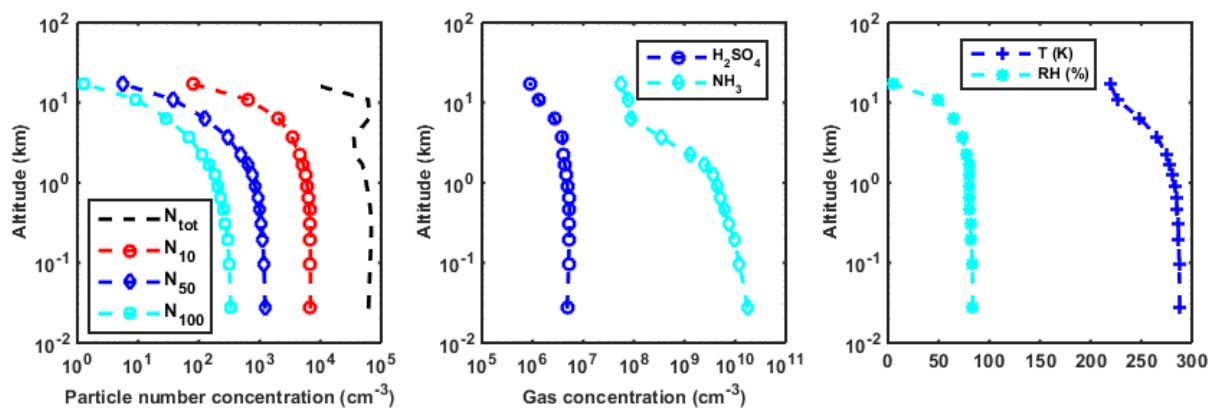
834

835 Figure 2. Comparison of predicted vs. measured hourly averaged number concentration of
836 particles larger than 10 nm (N_{10}), 50 nm (N_{50}) and 100 nm (N_{100}) during May 2008 from the 7
837 EUSAAR measurement stations during the EUCAARI project. Lines corresponding to 1:1
838 (solid line), and 1:2 and 2:1 (dashed lines) are shown. The PMCAMx-UF model simulation ACDC-
839 TUV-DE is used (see Table 1).

840

841

842

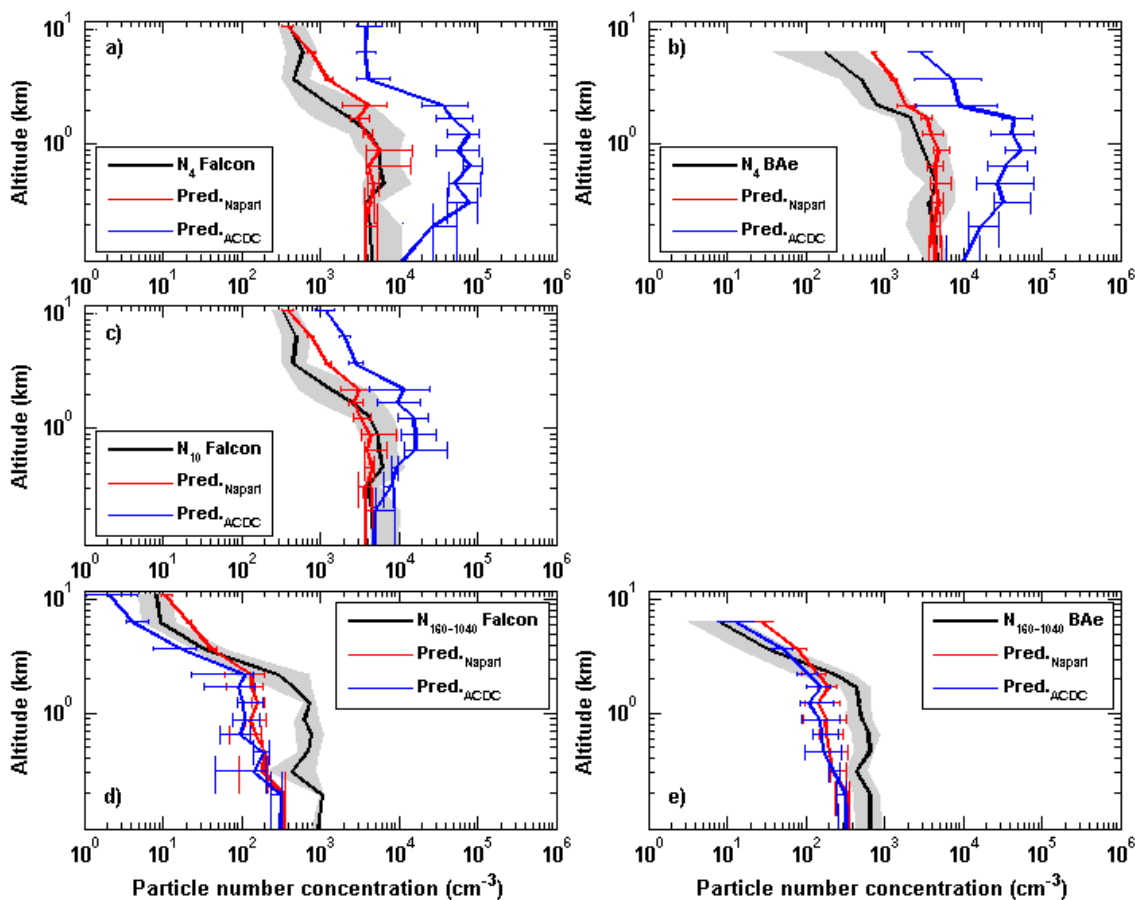


843

844 Figure 3. Vertical profiles of simulated variables averaged (arithmetic mean) over May 2008 and the
845 whole simulation domain. Left panel: number concentration (cm⁻³) of particles larger than 0.8 nm (N_{tot}),
846 10 nm (N_{10}), 50 nm (N_{50}) and 100 nm (N_{100}). Middle panel: gas phase concentration (cm⁻³) of sulfuric
847 acid (H_2SO_4) and ammonia (NH_3). Right panel: temperature (K) and relative humidity (%). The
848 PMCAMx-UF baseline simulation ACDC-TUV-DE is used (see Table 1).

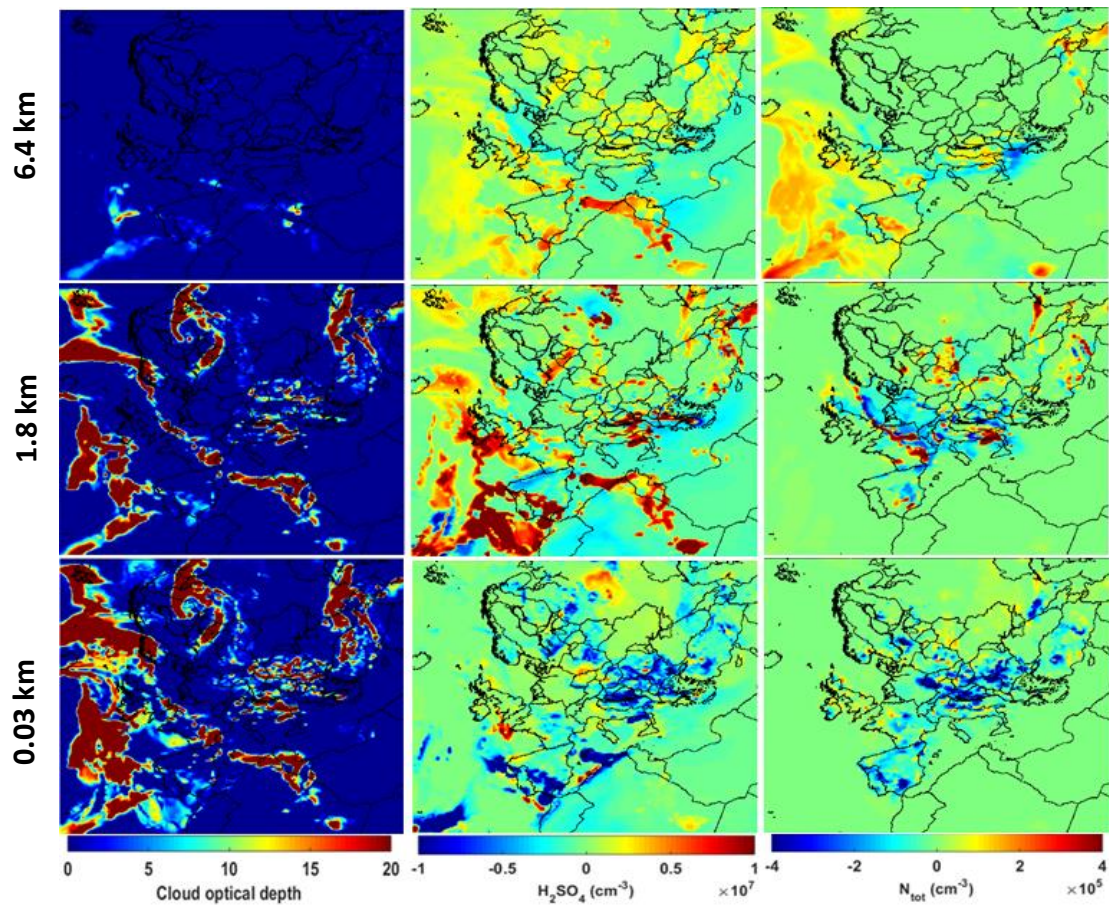
849

850
851
852



853
854
855
856
857
858
859
860
861
862
863
864
865
866

Figure 4. Vertical profiles of measured (black) and predicted (red and blue) particle number concentrations for the size ranges: (a) and (b) Larger than 4 nm (N_4) measurements collected by Falcon and BAe 146, respectively, (c) larger than 10 nm (N_{10}) measurements collected by Falcon 20, (d) and (e) 160-1040 nm ($N_{160-1040}$) measurements collected by Falcon and BAe 146, respectively, during May 2008. Red and blue lines show the predicted particle number concentrations by the PMCAMx-UF model using ACDC-based formation rates (ACDC-TUV-DE) and scaled Napari new particle formation scheme (Napari-TUV-DE), respectively. The lines show the median values of data points within each model layer, and the error bars and grey shading indicate the values between 25-th and 75-th percentiles of the model results and observations, respectively. Concentrations are given at ambient temperature and pressure.



867

868 Figure 5. Left column: the total cloud optical depth supplied by WRF meteorology model. Middle
 869 column: the absolute difference between the predictions using the TUV (the simulation ACDC-TUV-
 870 DE; see table 1) and RADM (the simulation ACDC-RADM-DE) radiative-transfer schemes within
 871 PMCAMx-UF for H_2SO_4 concentration. Right column: absolute difference between prediction using
 872 TUV and RADM schemes for total particle number concentrations N_{tot} . The parameters shown in the
 873 figure are snapshots on May 5, 2008 12:00 UTC at model layers 1 (mid-point altitude 0.03 km), 9 (mid-
 874 point altitude 1.7 km) and 12 (mid-point altitude 6.4 km).

875